Check for updates

Received: 14 January 2022 | Revised: 24 May 2022 | Accepted: 2 June 2022

DOI: 10.1049/gtd2.12621

IET Generation, Transmission & Distribution

The Institution of Engineering and Technology WILEY

ORIGINAL RESEARCH

An application of four-wire grid-forming power inverter in unbalanced distribution network

Jéssica S. Döhler[1] | Raul P. Mota[2] | João Antônio G. Archetti[2] | Dalmo C. Silva Júnior[2] | Cecilia Boström[1] | Janaína G. Oliveira[1,2]

[1]Division of Electricity, Department of Electrical Engineering, Uppsala University, Sweden

[2]Multi-Platform Simulations Laboratory, Electrical Engineering Program, Federal University of Juiz de Fora, Juiz de Fora, MG, Brazil

Correspondence
Jéssica S. Döhler, Division of Electricity, Department of Electrical Engineering, Uppsala University, Sweden.
Email: jessica.santos@uu.se

Funding information
Interreg Dualports; Energimyndigheten; Conselho Nacional de Desenvolvimento Científico e Tecnológico (CNPq); StandUp for Energy; Fundação de Amparo à Pesquisa no Estado de Minas Gerais (FAPEMIG); Scientific and Technological Development; J. Gust. Richers fundation; Instituto Nacional de Energia Elétrica; Coordenação de Aperfeiçoamento de Pessoal de Nível Superior (CAPES)

Abstract

The modelling of a three-phase four-leg four-wire grid-forming inverter in a low voltage distribution system 18-bus European Cigré under unbalanced conditions in an autonomous distribution network is presented. The case study has two types of inverters control strategy: (i) grid-forming to supply all the system demand in the interval of the intentional supply interruption and (ii) grid-following to integrate photovoltaic renewable energy resources into power systems. The model suggests a control scheme with two loops: An inner current loop with a proportional-integral controller and an outer voltage loop with a proportional controller, both in the synchronous reference frame (dq0), in which dq-axis are decomposed in positive and negative sequences. Simulation results, carried out using the PSCAD software, showed the effectiveness of the suggested control strategy with smooth synchronization where the grid-forming inverter was able to form a network with an unbalanced degree lower than 2%, sinusoidal voltage and frequency within standard limits 49.5–50.5 Hz.

1 | INTRODUCTION

The growing interest in the use of clean technologies in the area of power generation has stimulated research and development of systems using Renewable Energy Sources (RES). This increase is the result of environmental issues related to concerns about the use of fossil fuels in power generation [1, 2]. With the development of the distributed generation and its incorporation in the electric power system, a concept called microgrid started, being able to operate as an autonomous network, either in parallel or in isolation from the main electrical network [3].

Different topologies and functions can be attributed to these microgrids, making it possible to significantly improve the confiability of the system. Controls that were previously maintained at the transmission level during abnormal circumstances, such as failures in the main network and scheduled maintenance can now be performed locally. The islanded microgrid concept makes it suitable to be installed in remote regions, in areas where connection to the grid is not advantageous and to increase the system reliability [4–6].

Despite the benefits obtained with the use of the microgrids, one of the biggest challenge is to guarantee the quality in the energy supply, highlighting the unbalanced voltage caused by unbalanced three-phase loads, or single-phase load connected to the system [7–9]. This irregular distribution of loads in the electrical network may cause overloads in different levels each phase, generating unbalanced voltages and currents, even if this network is balanced in terms of impedance and susceptance elements. In this way, an unbalanced system is a condition when the three phases in the system have different amplitude and/or different phase angles of 120° between them [10]. Main norms and recommendations establish expressions to calculate the voltage unbalance. The American National Standard Institute (ANSI) [11], limit the maximum voltage unbalance in 3%, while the International Electrotechnical Commission (IEC) [12] and Agência Nacional de Energia Elétrica [13] recommends that

This is an open access article under the terms of the Creative Commons Attribution-NonCommercial-NoDerivs License, which permits use and distribution in any medium, provided the original work is properly cited, the use is non-commercial and no modifications or adaptations are made.
© 2022 The Authors. *IET Generation, Transmission & Distribution* published by John Wiley & Sons Ltd on behalf of The Institution of Engineering and Technology

17518695, 2023, 2, Downloaded from https://ietresearch.onlinelibrary.wiley.com/doi/10.1049/gtd2.12621 by Uppsala University Karin Boye, Wiley Online Library on [23/02/2023]. See the Terms and Conditions (https://onlinelibrary.wiley.com/terms-and-conditions) on Wiley Online Library for rules of use; OA articles are governed by the applicable Creative Commons License

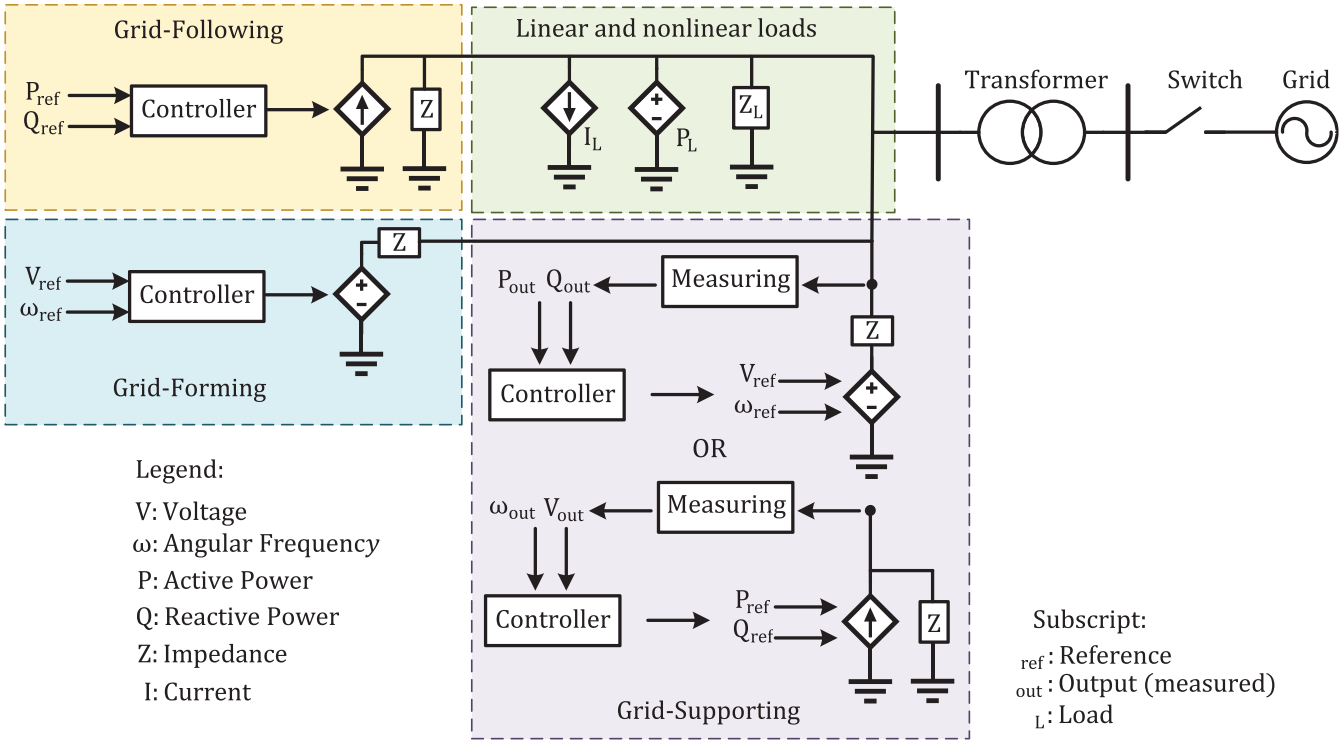

FIGURE 1 Grid-connected power electronics inverters modes

the voltage unbalance in the electric networks does not exceed 2%. Microgrids can be classified in terms of the type of bus, being Direct Current (DC), Alternating Current (AC) or hybrid (DC/AC). As for the AC type, a distributed unit can be classified into three groups in terms of control/inverter capacity: (i) Grid-Following (GFL) inverter (also called Grid-Feeding), (ii) Grid-Supporting (GSP) inverter and (iii) Grid-Forming (GFM) inverter [14, 15] as seen in Figure 1.

In most cases, the distribution systems are inserted in three-phase three-leg three-wire systems, not allowing the circulation of zero sequence current. However, three-phase four-leg four-wire inverters have grown considerably due to their ability to handle unbalanced loads and allow the inverter to compensate unbalanced voltage [16–19].

In this context, the three-phase four-leg four-wire inverters can operate flexibly in the grid-connected mode or the islanded mode, supporting the electric grid, complying with the power quality operational requirements. In the islanded mode, to keep the wave-forms within the standards, modelling and control techniques can be found in the literature. In [20], a cascade control strategy, Proportional Integral (PI) voltage and current loop referenced on the Synchronous Coordinates (dq0) are presented, where d and q axes are separated in negative and positive sequence. In [21], the strategy used consists of the independent control of the inverter phases based on four-leg buck inverter. In [22], a hierarchical control strategy with a primary and a secondary layer is proposed, consisting of a per-phase multi-loop control, Proportional (P) voltage and PI current loop, referenced on the $\alpha\beta$ coordinate. In [16], the control strategy consists of applying adaptive control to the system referenced on the dq0 frame.

Considering the references listed above, it is possible to notice that they lack a comprehensive model of the discussed cascade topology and the integration of multiple inverters between grid-forming and grid-following in a unbalanced distribution system. The present paper proposes such a contribution, using real data and a test system with larger number of buses. A control system with two loops is proposed: an inner current loop with PI controller and an outer voltage loop with P controller. As the voltage and the frequency are fixed in this case, the current will not be directly controllable but dependent on the load connected to the Common Coupling Point (PCC). Therefore this paper aims at bringing a novel and detailed modelling of three-phase four-leg four-wire grid-forming inverter, which can be used under island operation and unbalanced conditions. In order to achieve the objective of the proposed project, the modelling and control of GFL, connected to a photovoltaic solar generation unit and GFM is presented. Furthermore, a smooth resynchronization technique was applied. To show the effectiveness of the suggested control strategy, computer simulation results on PSCAD software with different scenarios are shown.

The paper is organized as follows: Section 2 is sub-divided into four parts: (i) System description, (ii) topology of low voltage distribution network 18-bus European Cigré, modelling and control of power electronics inverters, (iii) in GFL and (iv) GFM mode. Section 3 presents simulation results. Finally, concluding remarks are presented in Section 4.

17518695, 2023, 2, Downloaded from https://ietresearch.onlinelibrary.wiley.com/doi/10.1049/gtd2.12621 by Uppsala University Karin Boye, Wiley Online Library on [23/02/2023]. See the Terms and Conditions (https://onlinelibrary.wiley.com/terms-and-conditions) on Wiley Online Library for rules of use; OA articles are governed by the applicable Creative Commons License

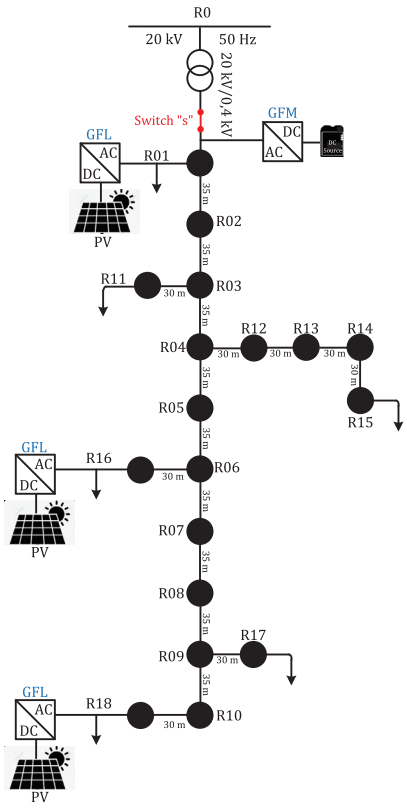

FIGURE 2 Study topology of low voltage distribution network 18-bus European Cigré

2 | METHODOLOGY

2.1 | System description

The system under study is a low voltage distribution system 18-bus European Cigré, which has four three-phase two-level Voltage Source Inverter (VSI) with two inverter control capacities: (i) GFL and (ii) GFM mode. The first configuration operates as a current source, controlling the currents to regulate the active and reactive powers when the microgrid is connected to the grid. The second configuration acts operating as a voltage source, imposing voltage and frequency on the AC bus, ensuring stability and operation of the islanded system. A schematic representation of the test system is shown in Figure 2.

Grid-connected photovoltaic systems are composed of PV arrays connected to the grid through power inverters and are designed to operate in parallel with the electric utility grid, as shown in Figure 2. The system is characterized as isolated mode when the switch "s" of the system is open, isolating the system from the main grid.

Low voltage distribution networks typically originate from a medium voltage/low voltage transformer, in this case, 20 kV/0.4 kV, and are of radial structure, as seen in Figure 2. Moreover, the size of the feeders is between 30 m to 35 m and the arrows in the system show the loaded buses. In bus-18 and bus-16, are inverters in the GFL mode connected and inverters in the GFM and GFL mode are connected to bus-1.

TABLE 1 Load parameters of low voltage distribution network [23]

Node	Apparent power [S](kVA)	Power factor (PF)
R1	200	0.95
R11	15	0.95
R15	52	0.95
R16	55	0.95
R17	35	0.95
R18	47	0.95

2.2 | System 18-bus European Cigré

Cigré 18-bus system is a European electrical distribution network configured for low voltage operation, containing short and underground feeders with balanced phases, whose nominal operation is 0.4 kV and 50 Hz. As it can be seen in Table 1, the system has a demand of 404 kVA and an inductive power factor of 0.95 [23].

The loads were considered balanced and modelled as constant impedance.

2.3 | Grid-following inverter (3 legs)

The inverter operating in the GFL mode supplies the grid with the maximum power extracted from the Distributed Generation (DG) unit. The electronic inverter acting as a grid-following, in most cases, has a fast current control, being seen by the AC grid, ideally, as a controlled AC current source [24].

One of the applications of these inverters is in the use of photovoltaic systems [25, 26]. Ideally, the photovoltaic solar cell is represented by a variable current source in parallel with a non-ideal diode, and it varies in a way directly proportional to the solar radiation incident on the cell plane.

In applications involving DG, it is usual to carry out the control of the current injected into the grid in order to control the active and reactive power exchange between the inverter and the electrical network. Two cascade control loops are usually implemented: (i) an external to control the voltage on the DC bus and (ii) an internal to output current control of the inverter. The cascade control loops and the main elements of GFL inverter mode are shown in Figure 3.

Considering a balanced AC grid, the three-phase currents can be calculated for each phase. Applying Kirchhoff's voltage law in the circuit, the following differential equation is obtained:

$$L_{L,abc}\frac{di_{abc,L}(t)}{dt} = -r_{L,abc}i_{abc,L}(t) + v_{t,abc}(t) - v_{s,abc}(t), \quad (1)$$

where $i_{abc,L}(t)$ are the three-phase output currents; $v_{t,abc}(t)$ are the terminal voltages of the inverter; $v_{s,abc}(t)$ are the AC voltages. Between the grid and the inverter output, there is impedance of a filter represented by $L_{L,abc}$ with intern resistence $r_{L,abc}$.

17518695, 2023, 2, Downloaded from https://ietresearch.onlinelibrary.wiley.com/doi/10.1049/gtd2.12621 by Uppsala University Karin Boye, Wiley Online Library on [23/02/2023]. See the Terms and Conditions (https://onlinelibrary.wiley.com/terms-and-conditions) on Wiley Online Library for rules of use; OA articles are governed by the applicable Creative Commons License

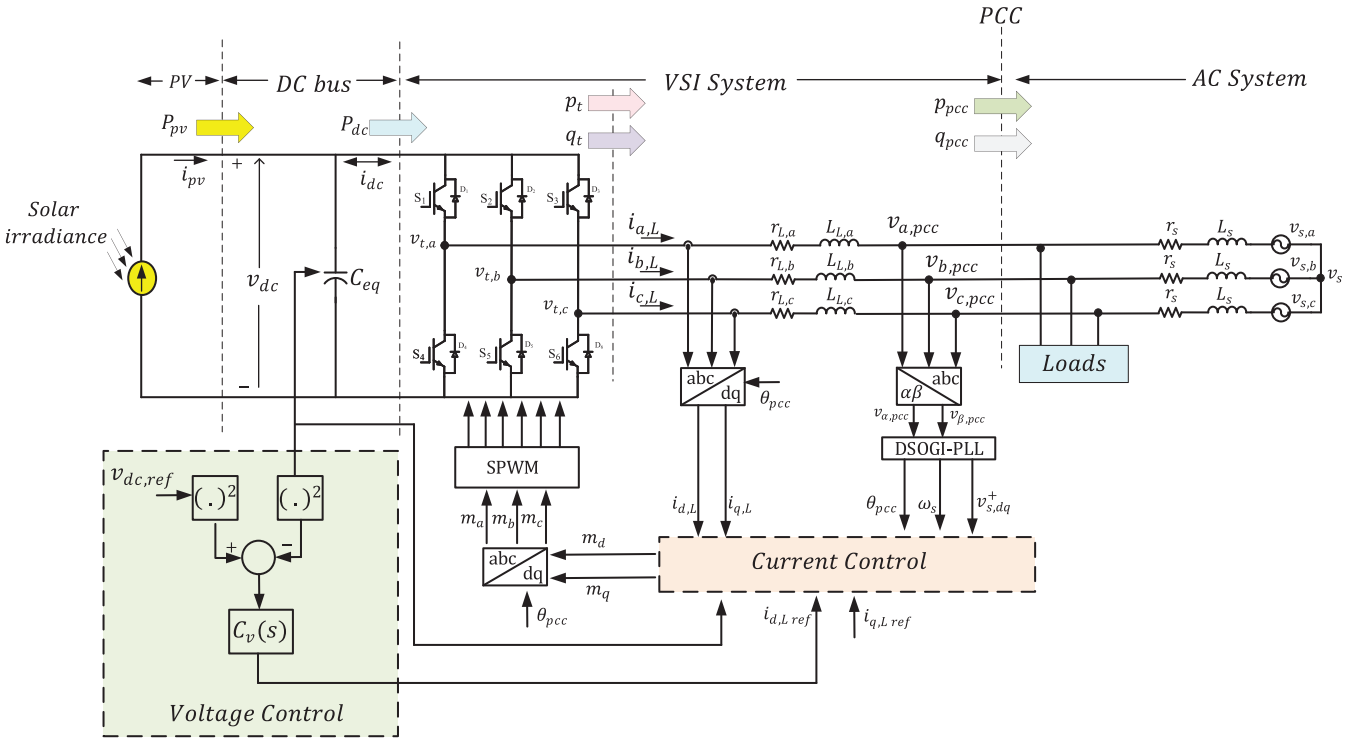

FIGURE 3 Block diagram of the control of the grid-following inverter

The transformation to the dq Park's frame of (1) lead to the following equations [27]:

$$\begin{cases} L_L \dfrac{di_{d,L}(t)}{dt} = L_L \omega i_{q,L}(t) - r_L\, i_{d,L}(t) + v_{t,d}(t) - v_{s,d}(t) \\ L_L \dfrac{di_{q,L}(t)}{dt} = -L_L \omega i_{d,L}(t) - r_L\, i_{q,L}(t) + v_{t,q}(t) - v_{s,q}(t) \end{cases}. \tag{2}$$

There is a cross-coupling between the direct axis and quadrature currents due to the terms $\omega i_{q,L}(t)$ and $\omega i_{d,L}(t)$, resulting from the transformation of the coordinate system. To synchronize the system is used Double Second Order Generalized Integrator PLL (DSOGI-PLL) which efficiently synchronizes the variables of the inverter with the local grid from the tracking of the phase angle of the electrical voltage at the PCC. Furthermore, a Sinosoidal Pulse Width Modulation (SPWM) technique is employed to obtain the required output current in the line side of the GFL inverter. The cascaded strategy use in both control loops a proportional-integral controller [27].

2.4 | Grid-forming inverter (4 legs)

The inverter operating in GFL mode has the voltage and frequency at the PCC imposed by grid, which does not occur in case of mains failure, operation in island mode, where the GFM inverters works by imposing voltage and frequency on the AC bus [28]. The performance of the output voltage control of inverter is evaluated according to the transient response time, steady state error and total harmonic distortion. For VSI to work correctly, a mathematical model of the plant is needed, suitable to be controlled. The mathematical model of the three-phase four-leg VSI with a LC filter, shown in Figure 4, in the dq0 is obtained as shown below.

From Figure 4, the voltage equations for the three phases (a,b,c) can be written, using the Kirchhoff voltage laws [16] as:

$$v_{jin}(t) = r_f i_j(t) + \frac{L_f di_j(t)}{dt} + v_{JN}(t) - \frac{L_f di_n(t)}{dt} - r_n i_n(t), \tag{3}$$

where the inductances of the coupling filter are the same, as well as their respective series resistances, that is, $(L_a = L_b = L_c = L_f)$ and $(r_a = r_b = r_c = r_f)$. Moreover $j \in \{a, b, c\}$ and $J \in \{A, B, C\}$.

Knowing (4) are valid in the case of unbalanced conditions.

$$i_n(t) = -(i_a(t) + i_b(t) + i_c(t)). \tag{4}$$

Derivative both sides of (4):

$$\frac{di_n(t)}{dt} = -\left(\frac{di_a(t)}{dt} + \frac{di_b(t)}{dt} + \frac{di_c(t)}{dt}\right). \tag{5}$$

17518695, 2023, 2, Downloaded from https://ietresearch.onlinelibrary.wiley.com/doi/10.1049/gtd2.12621 by Uppsala University Karin Boye, Wiley Online Library on [23/02/2023]. See the Terms and Conditions (https://onlinelibrary.wiley.com/terms-and-conditions) on Wiley Online Library for rules of use; OA articles are governed by the applicable Creative Commons License

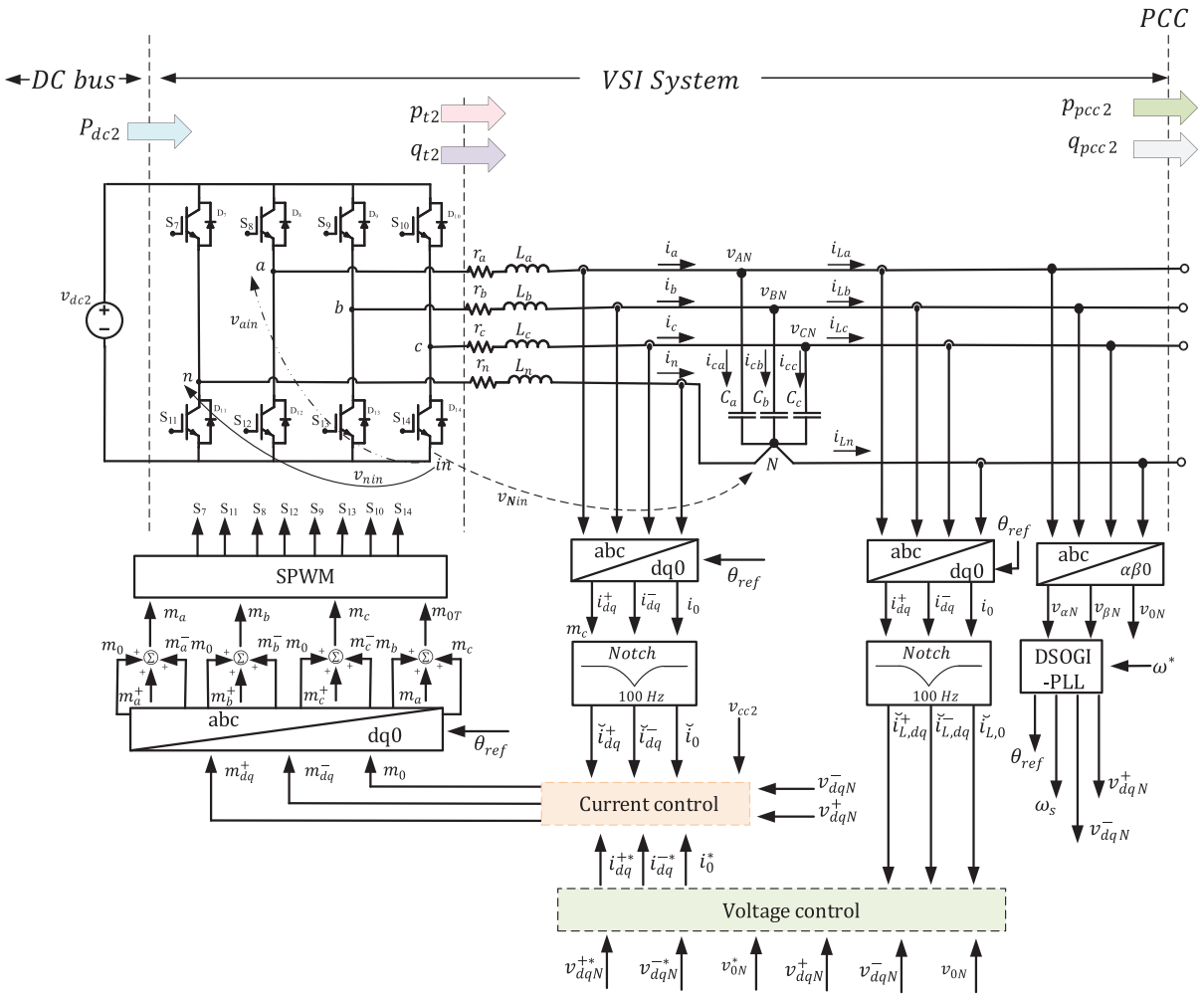

FIGURE 4 Block diagram of the control of the grid-forming inverter

Replacing (3) in (5) can be obtained:

$$\frac{di_n(t)}{dt} = -\frac{1}{4L_f}\left(v_{jin}(t) - v_{JN}(t) + 4r_f i_n(t)\right). \tag{6}$$

Expressions describing the dynamics of three-phase currents in an abc coordinate system in continuous-time state space equations are as in (7) and the intermediate steps come out in (3) through (6).

$$\frac{d}{dt}\begin{bmatrix} i_a(t) \\ i_b(t) \\ i_c(t) \end{bmatrix} = \overbrace{\frac{r_f}{L_f}\begin{bmatrix} -1 & 0 & 0 \\ 0 & -1 & 0 \\ 0 & 0 & -1 \end{bmatrix}}^{A}\begin{bmatrix} i_a(t) \\ i_b(t) \\ i_c(t) \end{bmatrix} + \overbrace{\frac{1}{4L_f}\begin{bmatrix} 3 & -1 & -1 \\ -1 & 3 & -1 \\ -1 & -1 & 3 \end{bmatrix}}^{B}\begin{bmatrix} v_{ain}(t) \\ v_{bin}(t) \\ v_{cin}(t) \end{bmatrix}$$
$$+ \overbrace{\frac{1}{4L_f}\begin{bmatrix} -3 & 1 & 1 \\ 1 & -3 & 1 \\ 1 & 1 & -3 \end{bmatrix}}^{F}\begin{bmatrix} v_{AN}(t) \\ v_{BN}(t) \\ v_{CN}(t) \end{bmatrix}, \tag{7}$$

where the state variables are the currents of the inverter $i_a(t)$, $i_b(t)$ and $i_c(t)$, the input voltages synthesized by the inverter $v_{ain}(t)$, $v_{bin}(t)$ e $v_{cin}(t)$ and as a disturbance the voltage of PCC $v_{AN}(t)$, $v_{BN}(t)$ and $v_{CN}(t)$.

The continuous time state-space model of a linear time-invariant system, as a function of the state variable vector $x(t)$, the input vector $u(t)$ and the disturbance vector $d(t)$, is:

$$\dot{x}(t) = Ax(t) + Bu(t) + Fd(t), \tag{8}$$

where $\dot{x}(t) = \begin{bmatrix} \dot{i}_a(t) & \dot{i}_b(t) & \dot{i}_c(t) \end{bmatrix}^\top$ is the state vector, $x(t) = \begin{bmatrix} i_a(t) & i_b(t) & i_c(t) \end{bmatrix}^\top$ is the state variable vector, $u(t) = \begin{bmatrix} v_{ain}(t) & v_{bin}(t) & v_{cin}(t) \end{bmatrix}^\top$ is the input vector and $d(t) = \begin{bmatrix} v_{AN}(t) & v_{BN}(t) & v_{CN}(t) \end{bmatrix}^\top$ is the disturbance vector.

In the above model, given in an abc coordinate system for four-leg currents, i_j(t) can be transformed into a $\alpha\beta0$ coordinates by using the 3 × 3 transformation matrix [29] $[T_{\alpha\beta0}]$ defined in (9). The inverse transformation matrix is given by Equation (10).

17518695, 2023, 2, Downloaded from https://ietresearch.onlinelibrary.wiley.com/doi/10.1049/gtd2.12621 by Uppsala University Karin Boye, Wiley Online Library on [23/02/2023]. See the Terms and Conditions (https://onlinelibrary.wiley.com/terms-and-conditions) on Wiley Online Library for rules of use; OA articles are governed by the applicable Creative Commons License

$$[T_{\alpha\beta0}] = \begin{bmatrix} 1 & -\frac{1}{2} & -\frac{1}{2} \\ 0 & \frac{\sqrt{3}}{2} & -\frac{\sqrt{3}}{2} \\ \frac{1}{2} & \frac{1}{2} & \frac{1}{2} \end{bmatrix}, \tag{9}$$

$$[T_{i,\alpha\beta0}] = \begin{bmatrix} 1 & 0 & 1 \\ -\frac{1}{2} & \frac{\sqrt{3}}{2} & 1 \\ -\frac{1}{2} & -\frac{\sqrt{3}}{2} & 1 \end{bmatrix}. \tag{10}$$

The vector of state variables $x(t)$, the input vector $u(t)$ and the disturbance vector $d(t)$, designed in the natural coordinates abc can be represented as shown in the equations (11), (12) and (13).

$$x(t) = [T_{i,\alpha\beta0}]x_{\alpha\beta0}(t), \tag{11}$$

$$u(t) = [T_{i,\alpha\beta0}]u_{\alpha\beta0}(t), \tag{12}$$

$$d(t) = [T_{i,\alpha\beta0}]d_{\alpha\beta0}(t), \tag{13}$$

where the state variable vector is $x_{\alpha\beta0}(t) = \begin{bmatrix} i_\alpha(t) & i_\beta(t) & i_0(t) \end{bmatrix}^\top$, the input vector is $u_{\alpha\beta0}(t) = \begin{bmatrix} v_{\alpha n}(t) & v_{\beta n}(t) & v_{0n}(t) \end{bmatrix}^\top$ and $d_{\alpha\beta0}(t) = \begin{bmatrix} v_{\alpha N}(t) & v_{\beta N}(t) & v_{0N}(t) \end{bmatrix}^\top$ is the disturbance vector.

Replacing Equation (8) with Equations (11), (12) and (13), and multiplying both sides by $[T_{\alpha\beta0}]$, we obtain:

$$\begin{aligned} &[T_{\alpha\beta0}][T_{i,\alpha\beta0}]\dot{x}_{\alpha\beta0}(t) \\ &= [T_{\alpha\beta0}]A[T_{i,\alpha\beta0}]x_{\alpha\beta0}(t) + [T_{\alpha\beta0}]B[T_{i,\alpha\beta0}]u_{\alpha\beta0}(t) \\ &\quad + [T_{\alpha\beta0}]F[T_{i,\alpha\beta0}]d_{\alpha\beta0}(t). \end{aligned} \tag{14}$$

Replacing the matrix of states defined in (7), (9) and (10) in (14), the term formed by the matrix of states for $\alpha\beta0$ system coordinate can be calculated by:

$$[T_{\alpha\beta0}]A[T_{i,\alpha\beta0}]x_{\alpha\beta0}(t) = \frac{3}{2}IAx_{\alpha\beta0}(t), \tag{15}$$

$$[T_{\alpha\beta0}]B[T_{i,\alpha\beta0}]u_{\alpha\beta0}(t) = \frac{3}{2}IB_{\alpha\beta0}u_{\alpha\beta0}(t), \tag{16}$$

$$[T_{\alpha\beta0}]F[T_{i,\alpha\beta0}]d_{\alpha\beta0}(t) = \frac{3}{2}IF_{\alpha\beta0}d_{\alpha\beta0}(t). \tag{17}$$

The state-space model is obtained for the $\alpha\beta0$ coordinates of three-phase four-leg inverter illustrated in Figure 4 as follows:

$$\dot{x}_{\alpha\beta0}(t) = Ax_{\alpha\beta0}(t) + Bu_{\alpha\beta0}(t) + Fd_{\alpha\beta0}(t), \tag{18}$$

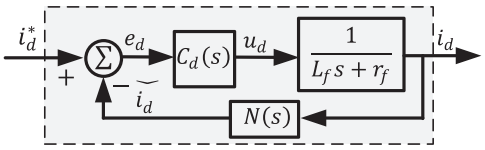

FIGURE 5 Positive sequence current control d-axis

$$\begin{aligned} \frac{d}{dt}\begin{bmatrix} i_\alpha(t) \\ i_\beta(t) \\ i_0(t) \end{bmatrix} &= \overbrace{\frac{r_f}{L_f}\begin{bmatrix} -1 & 0 & 0 \\ 0 & -1 & 0 \\ 0 & 0 & -1 \end{bmatrix}}^{A}\begin{bmatrix} i_\alpha(t) \\ i_\beta(t) \\ i_0(t) \end{bmatrix} + \overbrace{\frac{1}{4L_f}\begin{bmatrix} 4 & 0 & 0 \\ 0 & 4 & 0 \\ 0 & 0 & 1 \end{bmatrix}}^{B_{\alpha\beta0}}\begin{bmatrix} v_{\alpha n}(t) \\ v_{\beta n}(t) \\ v_{0n}(t) \end{bmatrix} \\ &\quad + \overbrace{\frac{1}{4L_f}\begin{bmatrix} -4 & 0 & 0 \\ 0 & -4 & 0 \\ 0 & 0 & -1 \end{bmatrix}}^{F_{\alpha\beta0}}\begin{bmatrix} v_{\alpha N}(t) \\ v_{\beta N}(t) \\ v_{0N}(t) \end{bmatrix}. \end{aligned} \tag{19}$$

As it can be seen from the dq0 models of the current in (20) given by matrix in [29], the dq-axis circuits are coupled through ωi_q and ωi_d, while the axis circuit is completely decoupled from the dq-axis circuits.

$$\begin{aligned} \frac{d}{dt}\begin{bmatrix} i_d(t) \\ i_q(t) \\ i_0(t) \end{bmatrix} &= \begin{bmatrix} -\frac{r_f}{L_f} & \omega & 0 \\ -\omega & \frac{1}{L_f} & 0 \\ 0 & 0 & -\frac{1}{L_f} \end{bmatrix}\begin{bmatrix} i_d(t) \\ i_q(t) \\ i_0(t) \end{bmatrix} + \begin{bmatrix} \frac{1}{L_f} & 0 & 0 \\ 0 & \frac{1}{L_f} & 0 \\ 0 & 0 & \frac{1}{4L_f} \end{bmatrix}\begin{bmatrix} v_{dn}(t) \\ v_{qn}(t) \\ v_{0n}(t) \end{bmatrix} \\ &\quad + \begin{bmatrix} -\frac{1}{L_f} & 0 & 0 \\ 0 & -\frac{1}{L_f} & 0 \\ 0 & 0 & -\frac{1}{4L_f} \end{bmatrix}\begin{bmatrix} v_{dN}(t) \\ v_{qN}(t) \\ v_{0N}(t) \end{bmatrix}. \end{aligned} \tag{20}$$

2.4.1 | Positive, negative and zero sequence current control

Figure 5 shows the block diagram of the positive sequence direct axis current controller. In this diagram, the variable u_d is the output of the direct axis compensator, which processes $e_d = i_d^* - i_d$ generating u_d, the process is similar to the quadrature axis [27]. Knowing that the variable to be controlled has a stationary characteristic, a PI controller can be used to ensure that the synthesized current tracks the reference signal without regime error. The transfer function of the PI controller is represented by $C_d(s)$. In addition, the current i_d passes through a Notch filter that rejects the second order harmonics, centered at the frequency of 100 Hz. This action has the purpose of eliminating the ripple superimposed on the DC value present in this variable due to the transformation of synchronous coordinates. Knowing that the variables to be controlled have a stationary characteristic, a PI controller can be used to ensure that the synthesized current tracks the reference signal without regime

17518695, 2023, 2, Downloaded from https://ietresearch.onlinelibrary.wiley.com/doi/10.1049/gtd2.12621 by Uppsala University Karin Boye, Wiley Online Library on [23/02/2023]. See the Terms and Conditions (https://onlinelibrary.wiley.com/terms-and-conditions) on Wiley Online Library for rules of use; OA articles are governed by the applicable Creative Commons License

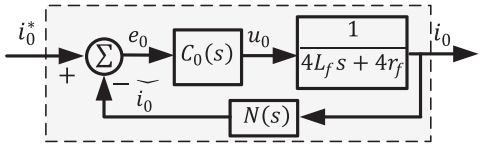

FIGURE 6 Zero sequence current control

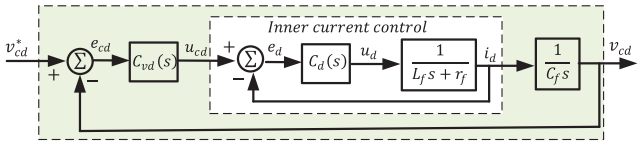

FIGURE 7 Diagram of direct axis voltage control

error. In this way, the PI gains of $C_d(s)$ are given by $k_{p,ip} = \frac{L_f}{\tau_i}$ and $k_{i,ip} = \frac{r_{L_f}}{\tau_i}$.

Different from the positive sequence current (dq-axis) controllers, that have the same dynamics, the current controller i_0 has a different dynamic response, being represented by the diagram shown in Figure 6. In this diagram, the variable u_0 is the output of the compensator that processes $e_0 = i_0^* - i_0$ generating u_0. The variable $v_{0N}(t)$ is used as a feed-forward signal. Similarly the PI gains of $C_0(s)$ are given by $k_{p,i0} = \frac{4L_f}{\tau_i}$ and $k_{i,i0} = \frac{4r_{L_f}}{\tau_i}$.

The control scheme of the negative sequence current used is similar to that of the positive sequence, differing in terms of cross-coupling that have opposite signs for the negative sequence due to the opposite rotation of the negative sequence. As a result, under unbalanced conditions, the negative sequence appears as a disturbance in components d and q, at a frequency of 2ω. This is because the frame of reference dq0 is rotating in the positive direction at an angular frequency of ω, while the negative sequence disturbance rotates at an angular frequency of ω in the opposite direction. Oscillations of 2ω in the measured signals can result in steady state errors when PI controller is used, since they track the reference signals, according to the principle of the internal model, (DC value). Oscillations must be canceled so that the injected currents can be fully controlled under unbalanced conditions. That is, this cancellation action has the purpose of eliminating the ripple superimposed on the DC value present in the dq0 variables due to the transformation of the abc coordinates to dq0. A Notch filter set to 2ω is suggested to be used to cancel these oscillations [30].

2.4.2 | AC voltage control

The VSI output voltages v_{AN}, v_{BN} and v_{CN}, which can be seen in Figure 4, is obtained using the Kirchhoff current law [16].

$$\frac{C_f dv_{JN}(t)}{dt} = i_{cj}(t) - i_{Lj}(t), \tag{21}$$

where the capacitances of the coupling filter are the same, ($C_a = C_b = C_c = C_f$). Moreover $j \in \{a, b, c\}$ and $J \in \{A, B, C\}$. The control of AC voltage in dq0 coordinates is similar to the process described in Section 2.4.1. The the output voltages of VSI in natural abc coordinates is transformed to $\alpha\beta 0$ coordinates and later in dq0. Therefore, as can be seen from the dq0 models of the voltage in (22) given by matrix in [29], the dq-axis circuits are coupled through ωv_q and ωv_d, while the 0-axis circuit is completely decoupled from the dq-axis circuits.

TABLE 2 GFL parameters

Parameter	Value
Filter resistances (r_L)	0.24 Ω
Filter inductances (L)	7.6 mH
DC submodule capacitance (C_{eq})	4700 uF
Switching frequency (f_{scL})	20 kHz
DC voltage (V_{α})	1000 V

$$\frac{d}{dt}\begin{bmatrix} v_{cd}(t) \\ v_{cq}(t) \\ v_{c0}(t) \end{bmatrix} = \begin{bmatrix} 0 & \omega & 0 \\ -\omega & 0 & 0 \\ 0 & 0 & 0 \end{bmatrix}\begin{bmatrix} v_{cd}(t) \\ v_{cq}(t) \\ v_{c0}(t) \end{bmatrix} + \begin{bmatrix} \frac{1}{C_f} & 0 & 0 \\ 0 & \frac{1}{C_f} & 0 \\ 0 & 0 & \frac{1}{C_f} \end{bmatrix}\begin{bmatrix} i_{dn}(t) \\ i_{qn}(t) \\ i_{0n}(t) \end{bmatrix}$$
$$+ \begin{bmatrix} -\frac{1}{C_f} & 0 & 0 \\ 0 & -\frac{1}{C_f} & 0 \\ 0 & 0 & -\frac{1}{C_f} \end{bmatrix}\begin{bmatrix} i_{Ldn}(t) \\ i_{Lqn}(t) \\ i_{L0n}(t) \end{bmatrix}. \tag{22}$$

As seen from the dq0 models of the current in (22) given by matrix in [29], the dq-axis circuits are coupled through ωv_q and ωv_d, while the axis circuit is completely decoupled from the dq-axis circuits.

Figure 7 shows the block diagram of the direct axis voltage controller. In this diagram, the variable u_{cd} is the output of the direct axis compensator, which processes $e_{cd} = v_{cd}^* - v_{cd}$ generating u_{cd}. The process is similar to the quadrature axis [27]. According to [31] the variable can be controlled as a stationary characteristic and a P controller can be used to ensure that the synthesized current tracks the reference signal. The transfer function of the controller P is represented by $C_{vd}(s)$. Therefore, the P gain of $C_{vd}(s)$ is given by $k_{p,v} = \frac{C_f}{\tau_v}$.

According to [31], the grid voltage time constant τ_v, used to calculate voltage control proportional gain $k_{p,v}$, is given by:

$$\tau_v = \frac{\sqrt{(\tan(M_p - \pi))^2 + 1}}{\omega_c \tan((M_p - \pi)}, \tag{23}$$

where the phase margin (M_p) is usually adopted at 60° and ω_c is equivalent to 20% or more of the maximum frequency equivalent to the harmonic to be compensated.

17518695, 2023, 2, Downloaded from https://ietresearch.onlinelibrary.wiley.com/doi/10.1049/gtd2.12621 by Uppsala University Karin Boye, Wiley Online Library on [23/02/2023]. See the Terms and Conditions (https://onlinelibrary.wiley.com/terms-and-conditions) on Wiley Online Library for rules of use; OA articles are governed by the applicable Creative Commons License

TABLE 3 GFL controllers parameters

Controller	Gain	Value
$C_i(s)$	$k_{p,is}$	15.2 $\frac{V}{A}$
	$k_{i,is}$	480 $\frac{V}{As}$
$C_v(s)$	$k_{p,vs}$	6.3294 10^{-4} $\frac{A}{V^2}$
	$k_{i,vs}$	0.0426 $\frac{A}{V^2 s}$

TABLE 4 GFM parameters

Parameter	Value
Filter resistances (r_f)	0.24 Ω
Filter inductances (L_f)	7.6 mH
Filter capacitance (C_f)	80 uF
Switching frequency (f_{scM})	20 kHz
DC voltage ($V_{\alpha 2}$)	2000 V

TABLE 5 GFM controllers parameters

Controller	Gain	Value
$C_d(s)$	$k_{p,ip}$	15.2 $\frac{V}{A}$
	$k_{i,ip}$	480 $\frac{V}{As}$
$C_0(s)$	$k_{p,i0}$	60.8 $\frac{V}{A}$
	$k_{i,i0}$	1920 $\frac{V}{As}$
$C_{vd}(s)$	$k_{p,v}$	0.12 $\frac{A}{V}$

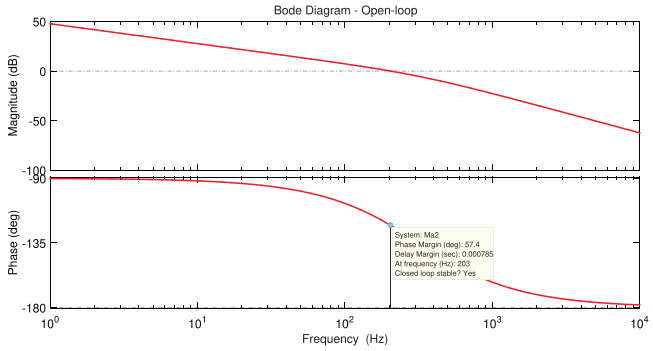

FIGURE 8 Positive and negative sequence bode diagram of the GFM open-loop transfer function

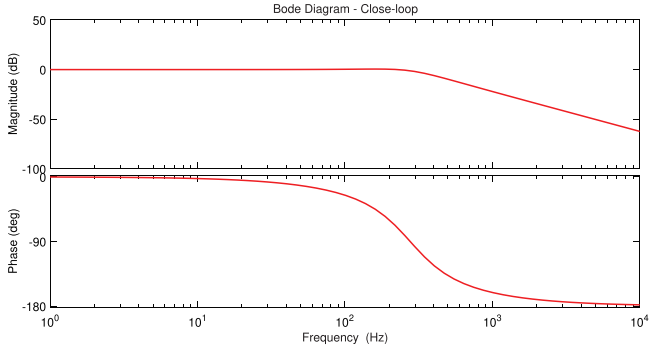

FIGURE 9 Positive and negative sequence bode diagram of the GFM close-loop transfer function.

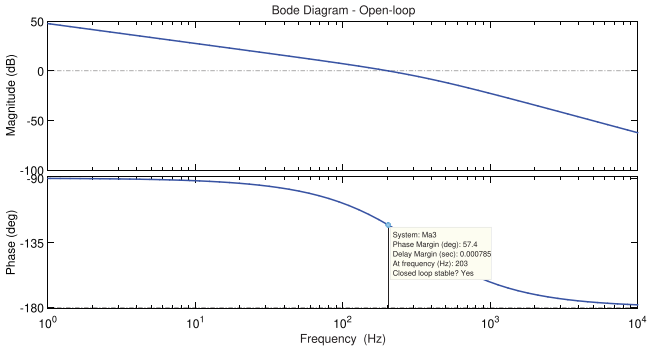

FIGURE 10 Zero sequence bode diagram of the GFM open-loop transfer function

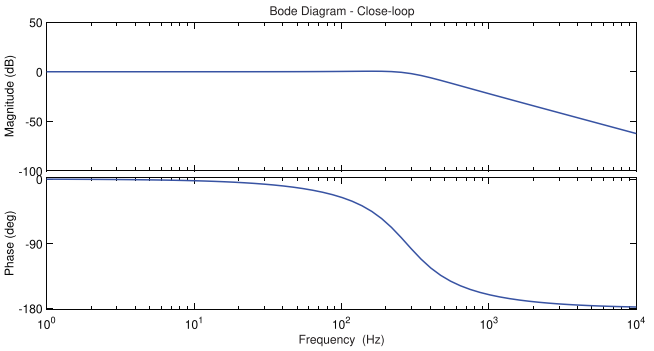

FIGURE 11 Zero sequence bode diagram of the GFM close-loop transfer function

For the zero sequence and negative sequence voltage control, the same strategy that was developed to positive sequence voltage control is adopted. However, for negative sequence, the dq0 transform signal will change, since the negative sequence rotates in the opposite direction of the positive sequence. The use of negative and zero sequence voltage loops will allow the inverter to form a balanced voltage, even though the system is composed of unbalanced lines. Therefore, the reference of the negative and zero sequence voltages will have their references set to zero.

3 | RESULTS

Simulations have been carried out using PSCAD software with focus on islanded operation mode and smooth synchronization in unbalanced conditions. The parameters of the inverters operating in the GFL mode connected to buses 18, 16 and 1 are presented in Table 2. The parameters of the controllers are given in Table 3. Moreover, parameters of the inverter operating in the GFM mode are presented in Table 4 and the parameters of the controllers are given in Table 5.

The following figures represent Bode's asymptotic tracing, which allows analyzing the stability of the control proposed for the system (Figure 4). There are two control loops in cascade configuration for the positive and negative sequences: A current loop representing the internal loop that regulates the i_d and i_q

17518695, 2023, 2, Downloaded from https://ietresearch.onlinelibrary.wiley.com/doi/10.1049/gtd2.12621 by Uppsala University Karin Boye, Wiley Online Library on [23/02/2023]. See the Terms and Conditions (https://onlinelibrary.wiley.com/terms-and-conditions) on Wiley Online Library for rules of use; OA articles are governed by the applicable Creative Commons License

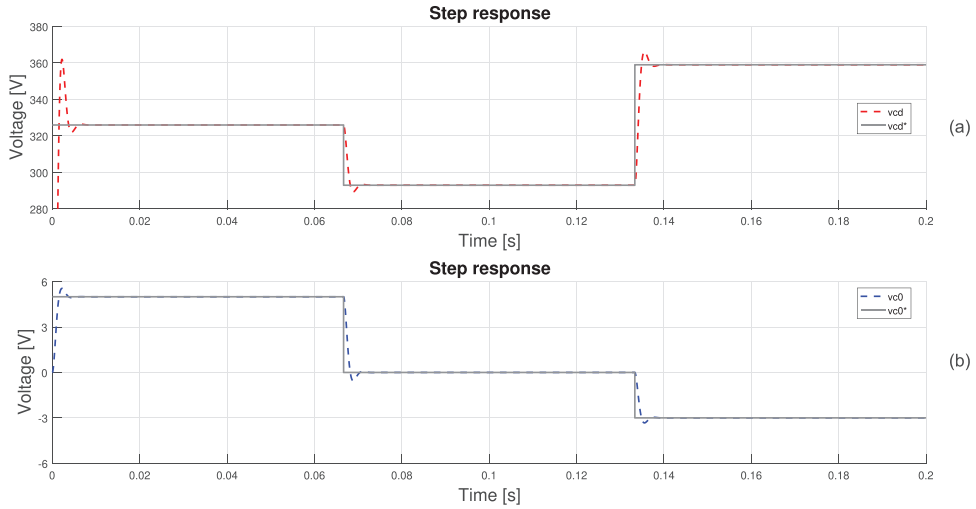

FIGURE 12 GFM voltage step response test: (a) Positive and negative sequence and (b) zero sequence

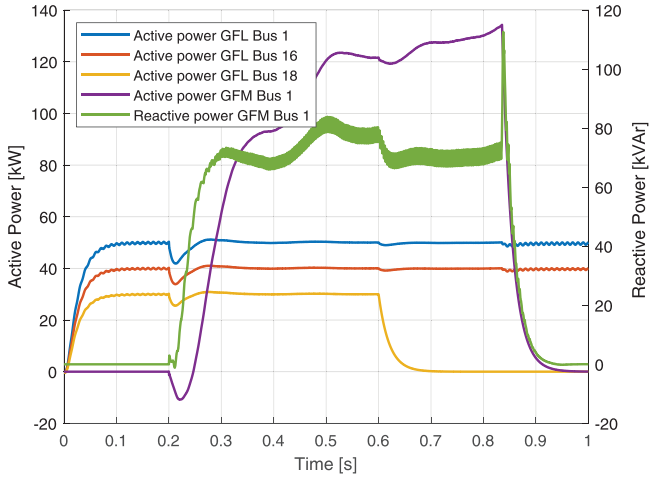

FIGURE 13 Powers of the system

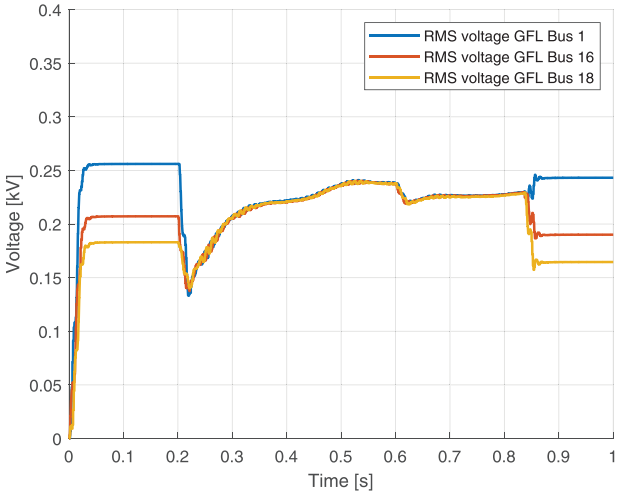

FIGURE 15 GFLs voltages

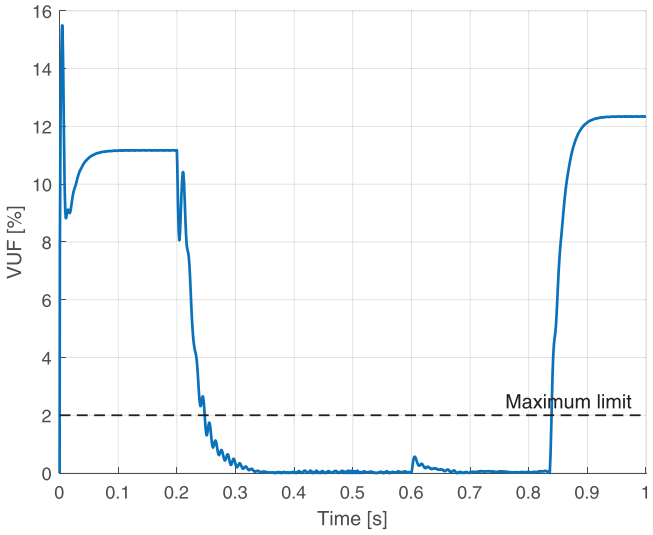

FIGURE 14 Voltage unbalanced factor

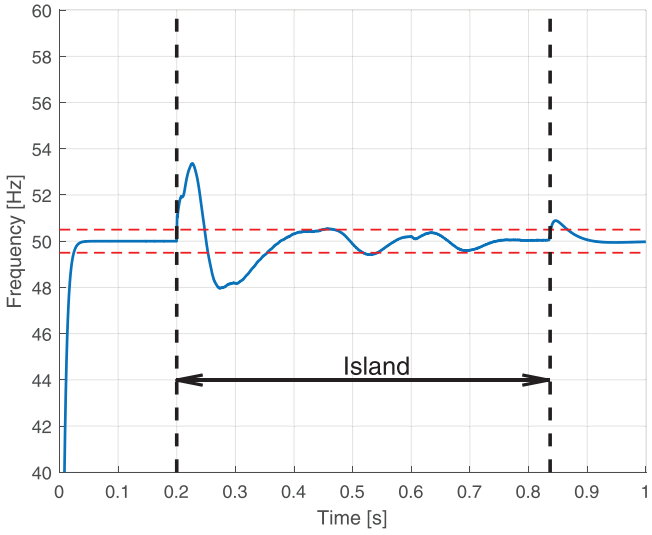

FIGURE 16 Frequency behavior in the grid-connected and isolated operation mode

17518695, 2023, 2, Downloaded from https://ietresearch.onlinelibrary.wiley.com/doi/10.1049/gtd2.12621 by Uppsala University Karin Boye, Wiley Online Library on [23/02/2023]. See the Terms and Conditions (https://onlinelibrary.wiley.com/terms-and-conditions) on Wiley Online Library for rules of use; OA articles are governed by the applicable Creative Commons License

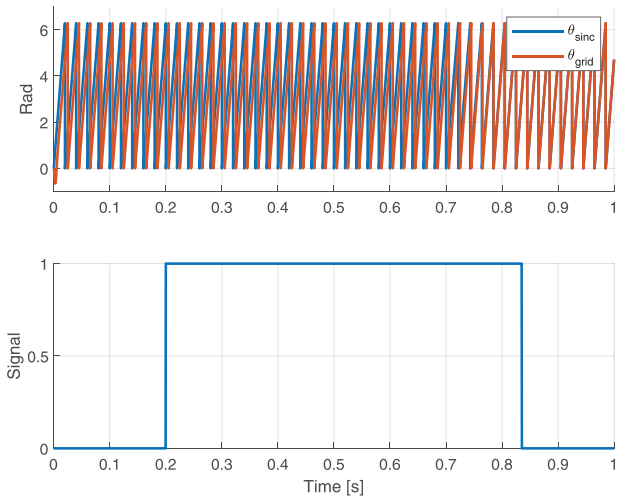

FIGURE 17 Smooth synchronization: (a) Theta angle and (b) switch "s" signal

currents and a voltage loop representing the outer loop that regulates the v_{cd} and v_{cq} voltages. The zero sequence has the same cascade configuration, but the inner loop regulates i_0 current and the outer loop regulates v_{c0} voltage.

Figures 8 and 10 represent the cascade control for positive, negative and zero sequences in open-loop for the system represented in Figure 7. In this system, the response of the plant and the controller are combined, excluding the effect of the feedback loop. Thus, it is noted that the system is stable as it has an infinite gain margin and phase margin approximately 60° as defined. Figures 9 and 11 represent the cascade control for the positive, negative and zero sequences in closed-loop for the system represented in Figure 7. In this system, the response of the plant and the controller are combined, including the effect of the feedback loop. As noted, the magnitude of the system is 0 dB which corresponds to the magnitude function of unity giving the maximum output. In other words, the output voltage is equal to the input voltage.

Figure 12 shows the step response of the system for voltage-tracking of the GFM inverter during islanded operation. It can be seen that required dynamics are achieved for the given time-domain specifications for positive, negative and zero sequence systems.

In order to raise the unbalance level, a factor was applied to all loads in the system, making the phases carry different current magnitudes, and the sum of the phase currents at the neutral point is not zero. The respectively load factors values used for phase a, b and c were 0.5, 0.6, and 0.7. Furthermore, the photovoltaic solar modules connected to the grid through a GFL inverter were represented by a current source where the converted solar energy is equivalent to 50 kW, 40 kW and 30 kW in buses 1, 16, and 18, respectively.

The following simulation tests of the low voltage distribution system have been proposed:

(i) System start (grid-connected);
(ii) t= 0.2 s intentional islanding;
(iii) t= 0.6 s removal GFL from bus 18;
(iv) t= 0.7 s return of the main grid.

When the switch "s" in Figure 2 is open in t= 0.2 s causing intentional islanding, the system loses voltage and frequency reference, in this way, GFM start providing these references. Due to this, the GFL proposed control strategy is capable to keeping injecting the power into the system. The output power waveforms of GFLs (active power production by PVs generators) and GFM (active and reactive power) can be seen in Figure 13.

In the grid-connected mode, the converters operate by importing and exporting energy from and to the power utility grid, ensuring power control flow, and supporting the grid through an array of ancillary services. On the other hand, in the islanded mode, at least one converter must function as a voltage source, providing grid voltage conditions and power quality of the microgrid. Thus, in islanded mode, there must be a balance between generation and demand so that deviations in voltage and frequency of the system is acceptable. Therefore, the active and reactive power injected by the converters must be consumed by the loads. In Figure 13, the active and reactive powers from GFM are zero before t= 0.2 s due to the operation in grid-connected mode. After t= 0.2 s, when the system start to work in isolated mode, the active and reactive power from the GFM start to increase to supply the load demand that was supplied by the main grid.

According to [13], the voltage unbalanced is analyzed based on the unbalanced factor, which expresses the relationship between the negative voltage sequence and positive voltage sequence components expressed in percentage terms of the positive sequence component at the PCC. This relation is given by the equation (24), having a value below the maximum limit of 2% during the regime.

$$VUF(\%) = \frac{\text{negative sequence voltage component}}{\text{positive sequence voltage component}} \cdot 100 \quad (24)$$

Therefore, it can be seen from Figure 14 that the voltage synthesized by the inverter has a high level of unbalance when the system is connected to the main grid. However, a small degree of unbalanced is seen during the isolated operation mode. This result shows the effectiveness of the suggested control strategy with smooth synchronization where the grid-forming inverter is able to form a network with an unbalanced degree lower than 2%, sinusoidal voltage and frequency within standard limits 49.5–50.5 Hz. In additional,the GFM is able to equilibrate the three phase voltage in the bus 1 as a result of unbalance voltage compensation, showing the effectiveness of the suggested control strategy suggested in this article, as seen in Figure 15.

When the generation unit from bus 18 is removed in $t = 0.6$ s, Figure 13 shows zero for the active power correspondent to GFL Bus 18. However, even with the disturbance caused in the system, the system is still below the maximum unbalance limit.

The voltage and frequency at PCC are related to the variations in active and reactive power of the network, seconds before islanding occurs [32]. When the system is islanded mode, in t = 0.2 s, the load controls the system's behavior. Before

17518695, 2023, 2, Downloaded from https://ietresearch.onlinelibrary.wiley.com/doi/10.1049/gtd2.12621 by Uppsala University Karin Boye, Wiley Online Library on [23/02/2023]. See the Terms and Conditions (https://onlinelibrary.wiley.com/terms-and-conditions) on Wiley Online Library for rules of use; OA articles are governed by the applicable Creative Commons License

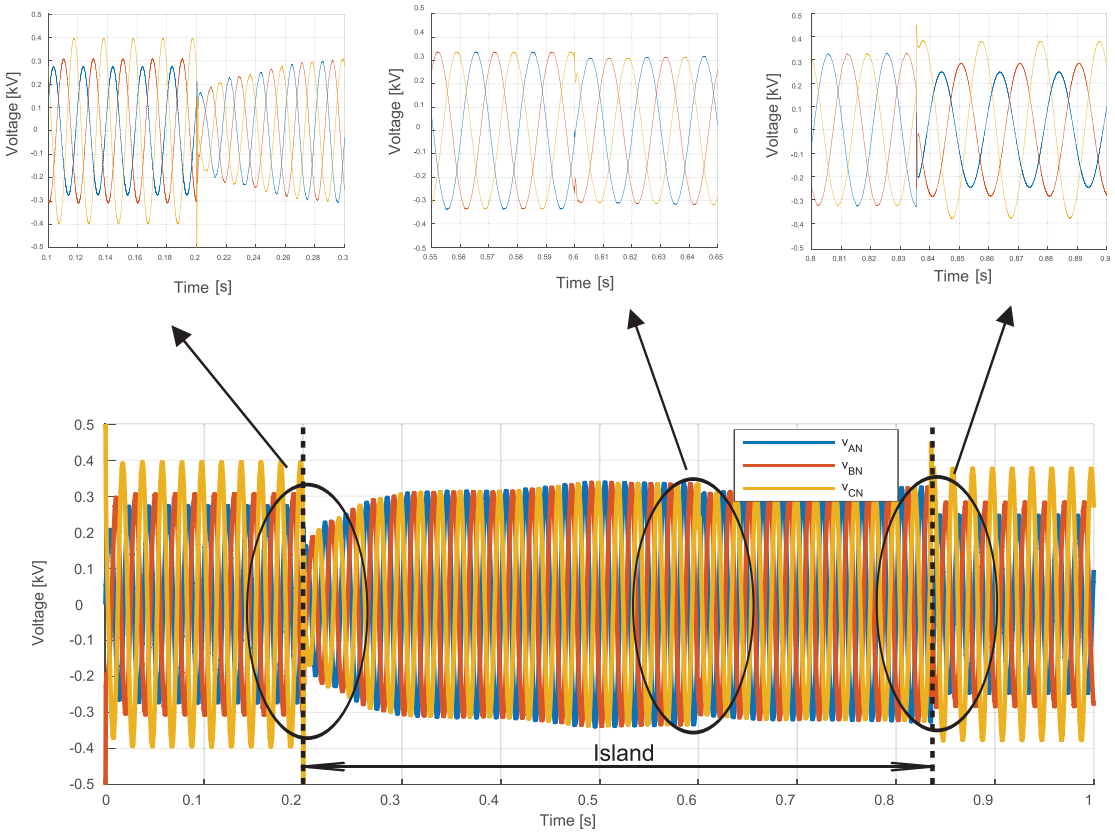

FIGURE 18 Three-phase voltage bus-1

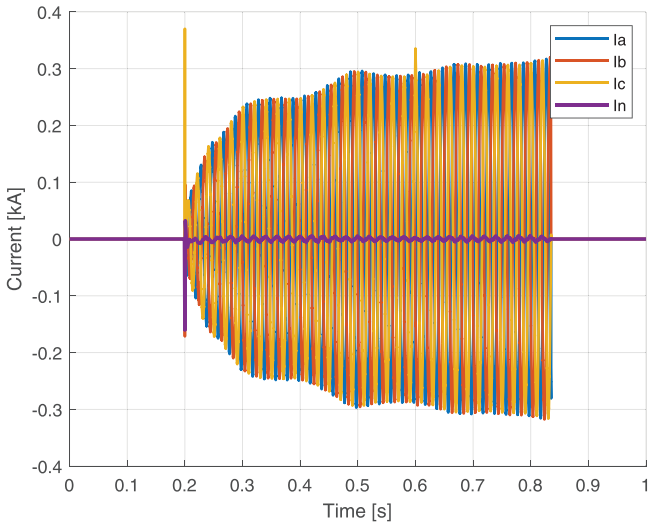

FIGURE 19 Grid-forming AC currents

intentional islanding, the loads demand 400 kVA from the grid. Due to this, there is a power variation at the PCC, once the solar panel is converting less active power than the demand load. In addition, the electrical network is injecting reactive power required by the load into the system. Due to the high variation in reactive power, right before islanding, the frequency value varied considerably. However, in steady state the frequency stabilizes at its nominal value of 50 Hz. The limits of 49.5–50.5 Hz are respected, as can be seen in Figure 16.

In $t = 0.6$ s, even with the disturbance caused in the system, the system is still within standard limits of frequency, as seen in Figure 16.

Due to the value of active power related to the load demand, the same occurs with the AC voltage, as seen in Figure 18. Therefore, it can be noted that voltage and frequency are dependent on the load behavior and the power balance of the system, before the opening of the switch "s".

In $t = 0.7$ s, the switch "s" is closed and the system is connected to main grid. However, the reconnection is performed only when the voltage synchronism between network and GFM are equal [33], which occurs at approximately $t = 0.8368$ s. It can be seen in Figure 17a,b which shows switch "s" signal during disconnection and connection of the system. During reconnection, a variation in frequency is seen, but after 0.1 s, the frequency stabilizes and starts operating within the standard limits.

When the system is islanded, the DG must be able to supply the active energy demand for the local load. However, if the generated power is not enough, then the voltage will fluctuate from the power drawn by the load. The same happens if the generated power is greater than the demand. Likewise, if the load's reactive power does not match the generated reactive power, the frequency in the PCC may also fluctuate, so it is important to maintain power balance. In the interval between $t = 0$ s and

17518695, 2023, 2, Downloaded from https://ietresearch.onlinelibrary.wiley.com/doi/10.1049/gtd2.12621 by Uppsala University Karin Boye, Wiley Online Library on [23/02/2023]. See the Terms and Conditions (https://onlinelibrary.wiley.com/terms-and-conditions) on Wiley Online Library for rules of use; OA articles are governed by the applicable Creative Commons License

$t = 0.2$ s, shown in Figure 19, it is noticed that the current of the grid-forming is zero since the system is operated in grid-connected mode. At $t = 0.2$ s, the islanded mode starts, as shown by the appearance of currents in the GFM. Due to the dynamic characteristic of the load connected to the system, the GFM's powers are not constant. Furthermore, in the interval of $t = 0.6$ s, the system suffers a loss of active power injection as the generating unit connected to GFL is removed from bus 18. Due to this, the grid-forming starts to inject more active power to supply the load demand, as can be seen in Figure 13. The current returning from neutral due to unbalance conditions remains the same when the GFL inverter was removed, as the unbalance only altered the three-phase power injection on three wires.

4 | CONCLUSIONS

This article proposed the use of a three-phase four-wire four-leg inverter connected to a low voltage distribution network 18-bus European Cigré system in order to provide the same nominal voltage and frequency conditions as the main feeder in island operation under unbalanced conditions. In addition, with the increase in the renewable energy generation, the electric power system has undergone changes, among them, the insertion of small energy generating units, close to the consumption center, in the subtransmission system and distribution. As a result, photovoltaic solar panels were connected to the system in order to reproduce this behavior in the electrical system. A comprehensive strategy of grid-forming converter was presented for compensating unbalanced currents and voltages in an islanded low voltage distribution system consisting of dispatchable units. The performance of the inverters was demonstrated by performing computer simulations using the PSCAD software, making it possible to validate the exposed models and controls during the article. From the simulation results, it is found that the proposed GFM control strategy can control voltage and frequency while maintaining them within their allowable limits with a low degree of unbalanced. Furthermore, it can be noted that voltage and frequency are dependent on the load behavior and the power balance of the system, before the intentional islanding. The proposed control strategy compensates positive, negative and zero sequence currents of unbalanced loads in a three-phase four-wire low voltage system, improving the power quality of the overall system.

AUTHOR CONTRIBUTIONS

Jéssica S. Döhler: Conceptualization, data curation, formal analysis, funding acquisition, investigation, methodology, project administration, resources, supervision, validation, visualization, writing - original draft, writing - review and editing. Raul Mota: Conceptualization, data curation, formal analysis, investigation, methodology, project administration, resources, supervision, validation, visualization, writing - original draft, writing - review and editing. Joao Archetti: Conceptualization, data curation, formal analysis, methodology, project administration, validation, visualization, writing - review and editing. Dalmo Cardoso: Conceptualization, formal analysis, methodology, project administration, validation, visualization, writing - review and editing. Cecilia Boström: Formal analysis, funding acquisition, project administration, visualization, writing - review and editing. Janaína G. Oliveira: Conceptualization, formal analysis, funding acquisition, methodology, project administration, validation, visualization, writing - review and editing.

ACKNOWLEDGEMENTS

Brazilian National Council is one funding and Coordination for the improvement of higher educationl personnel is another one.

The authors would like to give special thanks to Uppsala University, Vinnova, StandUp for Energy and Interreg Dual-ports, for Scientific and Technological Development, J. Gust. Richers foundation for funding, Swedish Energy Agency, Electrical Engineering Graduate Program and Federal University of Juiz de Fora, Electrical Engineering Graduate Program, Conselho Nacional de Desenvolvimento Científico e Tecnológico (CNPq), Coordenacão de Aperfeicoamento de Pessoal de Nivel Superior (CAPES), Fundação de Amparo á Pesquisa de Minas Gerais (FAPEMIG) and Instituto Nacional de Energia Elétrica (INERGE).

CONFLICTS OF INTEREST

The authors declare no conflict of interest.

DATA AVAILABILITY STATEMENT

Data sharing is not applicable to this article as no new data were created or analyzed in this study.

ORCID

Jéssica S. Döhler https://orcid.org/0000-0003-1571-1318

REFERENCES

1. Ogunrinde, O., Shittu, E., Dhanda, K.K.: Investing in renewable energy: Reconciling regional policy with renewable energy growth. IEEE Eng. Manage. Rev. 46, 103–111 (2018)
2. Qazi, A., Hussain, F., Rahim, N.A., Hardaker, G., Alghazzawi, D., Shaban, K., et al.: Towards sustainable energy: A systematic review of renewable energy sources, technologies, and public opinions. IEEE Access 7, 63837–63851 (2019)
3. Arfeen, Z.A., Khairuddin, A.B., Larik, R.M., Saeed, M.S.: Control of distributed generation systems for microgrid applications: A technological review. Int. Trans. Electr. Energy Syst. 29, e12072 (2019)
4. Wu, Y., Hu, M., Liao, M., Liu, F., Xu, C.: Risk assessment of renewable energy-based island microgrid using the hflts-cloud model method. J. Cleaner Prod. 284, 125362 (2021)
5. Qu, B., Shen, B., Shen, Y., Li, Q.: Dynamic state estimation for islanded microgrids with multiple fading measurements. Neurocomputing 406, 196–203 (2020)
6. Rodrigues, Y., Monteiro, M., Abdelaziz, M., Wang, L., de Souza, A.Z., Ribeiro, P.: Improving the autonomy of islanded microgrids through frequency regulation. Int. J. Electr. Power Energy Syst. 115, 105499 (2020)
7. Acharya, S., El.Moursi, M.S., Al.Hinai, A., Al.Sumaiti, A.S., Zeineldin, H.H.: A control strategy for voltage unbalance mitigation in an islanded microgrid considering demand side management capability. IEEE Trans. Smart Grid 10, 2558–2568 (2018)
8. Wang, Y., Zhou, G., Li, X.: A voltage unbalance compensation strategy based on virtual impedance for dgs in island microgrid without sequence component separation. Int. J. Electr. Power Energy Syst. 127, 106641 (2021)

17518695, 2023, 2, Downloaded from https://ietresearch.onlinelibrary.wiley.com/doi/10.1049/gtd2.12621 by Uppsala University Karin Boye, Wiley Online Library on [23/02/2023]. See the Terms and Conditions (https://onlinelibrary.wiley.com/terms-and-conditions) on Wiley Online Library for rules of use; OA articles are governed by the applicable Creative Commons License

9. Najafi, F., Hamzeh, M., Fripp, M.: Unbalanced current sharing control in islanded low voltage microgrids. Energies 11(10), 2776 (2018)
10. Tleis, N.: 2 - symmetrical components analysis of faulted three-phase networks containing voltage and current sources'. In: Tleis, N. (eds.) Power Systems Modelling and Fault Analysis, 2nd ed., pp. 41–99. Academic Press, London (2019). Available from: https://www.sciencedirect.com/science/article/pii/B9780128151174000023
11. American National Standard Institute (ANSI): ANSI Standard for Electric Power Systems and Equipment - Voltage Ratings (60 Hz) - c84. 1-2011. ANSI, New York (2011)
12. International Electrotechnical Commission (IEC): IEC 61000-3-13—electromagnetic compatibility (emc) - limits - assessment of emission limits for the connection of unbalanced installations to mv, hv and ehv power systems. IEC, Geneva (2008)
13. ANEEL: Agência nacional de energia elétrica-procedimentos de distribuição de energia elétrica no sistema elétrico nacional. Agência Nacional de Energia Elétrica (2012)
14. Antunes, H.M.A., Silva, S.M., Brandao, D.I., Machado, A.A.P., Ferreira, R.V.: A fault-tolerant grid-forming converter applied to ac microgrids. Int. J. Electr. Power Energy Syst. 121, 106072 (2020)
15. Rocabert, J., Luna, A., Blaabjerg, F., Rodríguez, P.: Control of power converters in AC microgrids. IEEE Trans. Power Electron. 27, 4734–4749 (2012)
16. Saim, A., Houari, A., Ahmed, M.A., Djerioui, A., Machmoum, M., Guerrero, J.M.: Adaptive reference trajectory for power quality enhancement in three-phase four-wire standalone power supply systems with nonlinear and unbalanced loads. IEEE J. Emerg. Sel. Topics Power Electron. 8, 1593–1603 (2020)
17. Doan, V.T., Kim, K.Y., Choi, W., Kim, D.W.: Design of a hybrid controller for the three-phase four-leg voltage-source inverter with unbalanced load. J. Power Electron. 17, 181–189 (2017)
18. Wang, R., Wang, F., Pan, H., Liu, S.: Hybrid pulse width modulation strategy of a high-frequency link three-phase four-leg matrix converter based on compensation theory. Appl. Sci. 10, 39 (2020)
19. Miveh, M.R., Rahmat, M.F., Ghadimi, A.A., Mustafa, M.W.: Control techniques for three-phase four-leg voltage source inverters in autonomous microgrids: A review. Renew. Sustain. Energy Rev. 54, 1592–1610 (2016)
20. Lliuyacc, R., Mauricio, J.M., Gomez.Exposito, A., Savaghebi, M., Guerrero, J.M.: Grid-forming vsc control in four-wire systems with unbalanced nonlinear loads. Electr. Power Syst. Res. 152, 249–256 (2017)
21. Yang, P., Ming, W., Liang, J., Wu, J.: A four-leg buck inverter for three-phase four-wire systems with the function of reducing dc-bus ripples. In: IECON 2019-45th Annual Conference of the IEEE Industrial Electronics Society, vol. 1, pp. 1508–1513. IEEE, Piscataway (2019)
22. Naderipour, A., Abdul.Malek, Z., Ramachandaramurthy, V.K., Kalam, A., Miveh, M.R.: Hierarchical control strategy for a three-phase 4-wire microgrid under unbalanced and nonlinear load conditions. ISA Trans 94, 352–369 (2019)
23. Barsali, S., et al.: Benchmark systems for network integration of renewable and distributed energy resources (2014)
24. Chhor, J., Sourkounis, C.: Optimal voltage control strategy for grid-feeding power converters in ac microgrids. Electr. Power Syst. Res. 176, 105945 (2019)
25. Hassaine, L., Bengourina, M.R.: Control technique for single phase inverter photovoltaic system connected to the grid. Energy Rep. 6, 200–208 (2020)
26. Zeb, K., Uddin, W., Khan, M.A., Ali, Z., Ali, M.U., Christofides, N., et al.: A comprehensive review on inverter topologies and control strategies for grid connected photovoltaic system. Renew. Sustain. Energy Rev. 94, 1120–1141 (2018)
27. Yazdani, A., Iravani, R.: Voltage-sourced converters in power systems: modeling, control, and applications, 1st ed. John Wiley & Sons, Hoboken, NJ (2010)
28. Rosso, R., Engelken, S., Liserre, M.: Robust stability investigation of the interactions among grid-forming and grid-following converters. IEEE J. Emerg. Sel. Topics Power Electron. 8, 991–1003 (2019)
29. O'Rourke, C.J., Qasim, M.M., Overlin, M.R., Kirtley, J.L.: A geometric interpretation of reference frames and transformations: dq0, clarke, and park. IEEE Trans. Energy Convers. 34, 2070–2083 (2019)
30. Duarte, S.N., Souza, B.C., Almeida, P.M., Araujo, L.R., Barbosa, P.G.: Control algorithm for dstatcom to compensate consumer-generated negative and zero sequence voltage unbalance. Int. J. Electr. Power Energy Syst. 120, 105957 (2020)
31. Barragán Villarejo, M., Mauricio, J.M., Olives Camps, J.C., Matas Díaz, F.J., de Paula García López, F., Maza Ortega, J.M.: Harmonic and imbalance compensation in grid-forming vsc. In: 2020 IEEE International Conference on Industrial Technology (ICIT), pp. 757–762. IEEE, Piscataway (2020)
32. Shetty, N.: An overview of islanding detection methods in photovoltaic systems copy (2011)
33. Alves, A.G.P.: Controle e ressincronização de uma microrrede ilhada com validação em protótipo de escala reduzida. Universidade Federal do Rio de Janeiro (2018)

How to cite this article: Döhler, J.S., Mota, R.P., Archetti, J.A.G., Júnior, D.S., Boström, C., Oliveira, J.G.: An application of four-wire grid-forming power inverter in unbalanced distribution network. IET Gener. Transm. Distrib. 17, 324–336 (2023). https://doi.org/10.1049/gtd2.12621

17518695, 2023, 2, Downloaded from https://ietresearch.onlinelibrary.wiley.com/doi/10.1049/gtd2.12621 by Uppsala University Karin Boye, Wiley Online Library on [23/02/2023]. See the Terms and Conditions (https://onlinelibrary.wiley.com/terms-and-conditions) on Wiley Online Library for rules of use; OA articles are governed by the applicable Creative Commons License